南京大學 NANJING UNIVERSITY | 非微扰物理研究所 Institute for Nonperturbative Physics

Backward DVCS in a Sullivan Process

Institute for Nonperturbative Physics

Abigail R. Castro

Nanjing University

arcastro@nju.edu.cn

Phys. Rev. D **112**, 034009 (2025)

In collaboration with: C. Mezrag · J. M. Morgado Chávez · B. Pire

Outline

1. **Motivation and the Sullivan process**
   Forward, backward and Bethe–Heitler mechanisms.
2. **Pion-to-photon transition distribution amplitudes**
   Operator definitions and partonic interpretation.
3. **Building blocks of the model**
   Pion and photon light-front wave functions.
4. **Constructing TDAs: from DGLAP to ERBL**
   Overlap representation and covariant extension.
5. **TDA predictions and QCD evolution**
   Vector and axial distributions, sum rules and scale dependence.
6. **Phenomenology and outlook**
   Cross sections, pion and rho channels, and experimental prospects.

Motivation

Can backward Sullivan scattering probe the nonperturbative photon content of the pion?

- **Strong-interaction dynamics in a photon transition.**
  Pion-to-photon TDAs connect the quark structure of a strongly bound meson to a real photon.
- **A complementary view of pion structure.**
  These transition correlations complement pion GPDs and retain parton-momentum information integrated out in radiative transition form factors.
- **A route to experimental access.**
  The Sullivan process provides access to a pion target, while backward exclusive channels probe its axial and vector photon-transition correlations.

This work: connect pion–photon correlations
to quantitative predictions for backward observables.

The Sullivan process

Sullivan process: a hard probe scatters from a virtual pion emitted by the proton, $p \to n + \pi^+$, providing access to pion structure.

Sullivan, PRD 5, 1732 (1972); Castro et al., Sec. III; Amrath–Diehl–Lansberg, EPJC 58, 179 (2008).

Forward DVCS

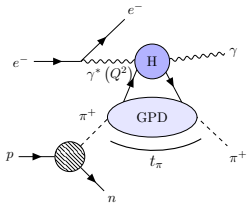

Small $|t_\pi|$: pion GPD.

Backward DVCS

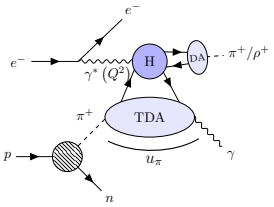

Small $|u_\pi|$: $\pi \to \gamma$ TDA.

Bethe–Heitler (BH)

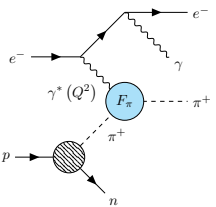

Real photon emitted by a lepton.

DVCS: deeply virtual Compton scattering, $\gamma^* \pi \to \gamma \pi$.

Collinear Factorisation

At large Q^2, the amplitude factorises into a perturbative hard kernel and a soft non-perturbative kernel.

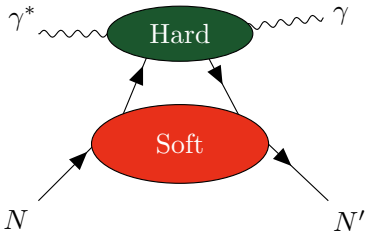

The external states select the class of the soft kernel.

- Small $|t|$: **GPDs**. Factorisation proven to all orders.
- Small $|u|$: **TDAs**. No all-orders proof; assumed by analogy.

Collins and Freund, PRD 59, 074009 (1999)

Collinear Factorisation

At large Q^2, the amplitude factorises into a perturbative hard kernel and a soft non-perturbative kernel.

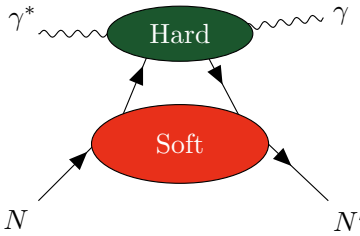

The external states select the class of the soft kernel.

- Small $|t|$: **GPDs**. Factorisation proven to all orders.
- Small $|u|$: **TDAs**. No all-orders proof; assumed by analogy.

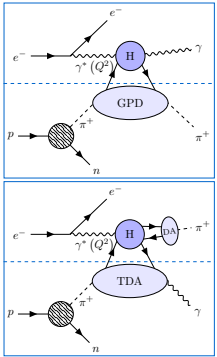

Collins and Freund, PRD 59, 074009 (1999)

Forward and backward scattering

Directions in the $\gamma^*\pi$ centre-of-mass frame

Near forward: $\theta_\gamma \simeq 0$

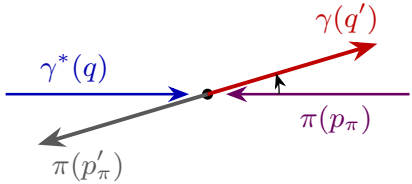

$t_\pi = (q - q')^2, \qquad |t_\pi| \ll Q^2, s_\pi.$

The real photon follows the hard probe.
The pion remains in the soft GPD transition.

Near backward: $\theta_\gamma \simeq \pi$

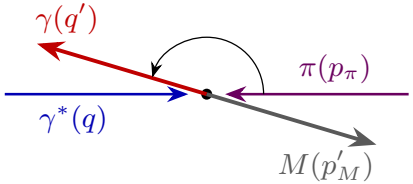

$u_\pi = (q' - p_\pi)^2, \qquad |u_\pi| \ll Q^2, s_\pi.$

The real photon follows the incoming pion.
The hard subprocess produces the outgoing meson.

$s_\pi = (q + p_\pi)^2$; the angle is measured from the incoming γ^* direction.

Factorization selects the nonperturbative object

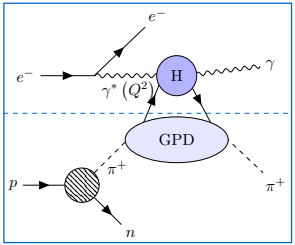

$$\mathcal{M}_{\text{fwd}} \sim C \otimes H_\pi$$

A pion GPD connects the initial and final pion.

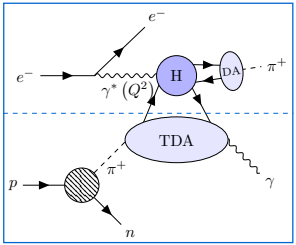

$$\mathcal{M}_{\text{bwd}} \sim \Phi_M \otimes C \otimes T^{\pi\gamma}$$

A pion-to-photon TDA accompanies the outgoing-meson distribution amplitude.

Working hypothesis: leading-twist backward factorization and longitudinal virtual-photon dominance; no general all-orders proof is supplied for this channel.

Castro et al., Sec. III; Collins and Freund, PRD 59, 074009 (1999), for forward DVCS.

Pion-to-photon TDA: definition and light-front ingredients

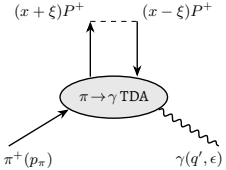

A two-parton correlation between a pion and a real photon:

$$\mathcal{F}_\Gamma(x,\xi,u) = \frac{1}{2}\int \frac{dz^-}{2\pi}\, e^{ixP^+z^-} \times \langle \gamma(q',\epsilon)|\bar{d}(-z/2)\,\Gamma\,\mathcal{W}\,u(z/2)|\pi^+(p_\pi)\rangle\big|_{z^+=z_\perp=0}.$$

Axial: $\Gamma=\gamma^+\gamma_5 \;\to\; A^{\pi\gamma}$; **vector:** $\Gamma=\gamma^+ \;\to\; V^{\pi\gamma}$.

Pion LFWFs: Bethe–Salpeter projection

$$\psi^\pi_{\uparrow\downarrow}(X,k_\perp) = N_\pi \frac{M^3 X(1-X)}{(k_\perp^2+M^2)^2},$$

$$ik_\perp \psi^\pi_{\uparrow\uparrow}(X,k_\perp) = N_\pi \frac{k_\perp M^2 X(1-X)}{(k_\perp^2+M^2)^2},$$

$$N_\pi = \frac{8\sqrt{15}\pi}{\sqrt{N_c}}, \qquad M = 318\,\text{MeV}.$$

Photon LFWFs: tree-level quark–photon vertex

$$\psi^\gamma_{\gamma\cdot n}(X,k_\perp) = -\frac{1-2X}{k_\perp^2+M^2},$$

$$\psi^\gamma_{\gamma\cdot n\gamma_5}(X,k_\perp) = \frac{1}{k_\perp^2+M^2},$$

$$\psi^\gamma_{\sigma n_\perp}(X,k_\perp) = \frac{iM}{k_\perp^2+M^2}.$$

LF kinematics: $P=(p_\pi+q')/2, \Delta=q'-p_\pi, u=\Delta^2, \xi=-\Delta^+/(2P^+); k^+_{\text{in/out}}=(x\pm\xi)P^+$.

Wilson line: $\mathcal{W}^\dagger\mathcal{W}=1$ (unitary QCD gauge link); the straight link becomes $\mathcal{W}=1$ in light-cone gauge $A^+=0$.

Pion LFWFs: from the covariant model to the light front

Euclidean algebraic model: chiral limit $p^2 = 0$, with $\nu = 1$.

$$\chi^{\rm sym}_{\pi,E}(\ell, p) = S_E(\ell + p/2)\, \Gamma^{\rm sym}_{\pi,E}(\ell, p)\, S_E(\ell - p/2).$$

1. Propagator and pion vertex

$$S_E(k) = \frac{-i\gamma\cdot k + M}{k^2 + M^2},$$

$$n_\pi \Gamma^{\rm sym}_{\pi,E}(\ell, p) = i\gamma_5 \int_{-1}^{1} dz\, \rho_1(z) \frac{M^2}{\ell_z^2 + M^2},$$

$$\ell_z = \ell + \frac{z}{2}p, \qquad \rho_1(z) = \frac{3}{4}(1 - z^2).$$

2. Formal light-front projection

$$\psi^\pi_{\uparrow\downarrow} \propto \int \frac{d\ell^-}{2\pi}\, {\rm Tr}[\gamma^+ \gamma_5 \chi^{\rm sym}_{\pi,M}],$$

$$ik^j_\perp \psi^\pi_{\uparrow\uparrow} \propto \int \frac{d\ell^-}{2\pi}\, {\rm Tr}[\sigma^{+j} \gamma_5 \chi^{\rm sym}_{\pi,M}].$$

$\ell^+ = (x - 1/2)p^+, \ell_\perp = k_\perp, p_\perp = 0.$

Project the Minkowski continuation $\chi_{\pi,M}$.

3. Normalised LFWFs used in the TDA model

$$\psi^\pi_{\uparrow\downarrow}(x, k_\perp) = N_\pi \frac{M^3 x(1-x)}{(k_\perp^2 + M^2)^2}, \qquad ik_\perp \psi^\pi_{\uparrow\uparrow}(x, k_\perp) = N_\pi \frac{k_\perp M^2 x(1-x)}{(k_\perp^2 + M^2)^2}.$$

$N_\pi = 8\sqrt{15}\pi/\sqrt{N_c}$; $M = 318$ MeV is fixed by the pion electromagnetic charge radius.

Helicity content: anti-aligned quarks have $L_z = 0$; aligned quarks require $k_1 \pm ik_2$ factors, with $|L_z| = 1$.

Mezrag et al., PLB 741, 190 (2015), Eq. (15); FBS 57, 729 (2016), Eqs. (79)–(83), (151)–(153); Chouika et al., PLB 780, 287 (2018), Eqs. (20)–(22)

Photon LFWFs from the LO quark–photon vertex

1. Photon $q\bar{q}$ component: a pointlike vertex $\Gamma^{\mu}_{\gamma,0} = \gamma^{\mu}$ (charge factored out).

$$\chi^{\lambda}_{\gamma,M}(\ell, q') = S_M(\ell + q'/2)\,(\gamma\cdot\epsilon_\lambda)\,S_M(\ell - q'/2), \qquad q'^2 = 0.$$



Same effective quark mass as for the pion:

$$M = 318\,\text{MeV}.$$

2. Light-front projection

$$\mathcal{C}^{\lambda}_{\Gamma}(x, k_\perp) = \int \frac{d\ell^-}{2\pi}\ \mathrm{Tr}\Big[\Gamma \chi^{\lambda}_{\gamma,M}(\ell, q')\Big].$$

$$\Gamma \in \{\not{n},\ \not{n}\gamma_5,\ \sigma^{n\perp}\}.$$

$\ell^+ = (x - \frac{1}{2})q'^+, \ell_\perp = k_\perp, q'_\perp = 0.$

The calculation reconstructs the x dependence from Mellin moments.

3. Scalar LFWFs used in the TDA overlap

$$\psi^{\gamma}_{\not{n}} = -\frac{1-2x}{k_\perp^2 + M^2}, \qquad \psi^{\gamma}_{\not{n}\gamma_5} = \frac{1}{k_\perp^2 + M^2}, \qquad \psi^{\gamma}_{\sigma^{n\perp}} = \frac{iM}{k_\perp^2 + M^2}.$$

The spin, polarisation, charge and normalisation factors are carried by the photon Fock states.

Ball, Braun and Kivel, NPB 649, 263 (2003), Sec. 2.2, Eqs. (2.21)–(2.22)

Partonic support: DGLAP and ERBL

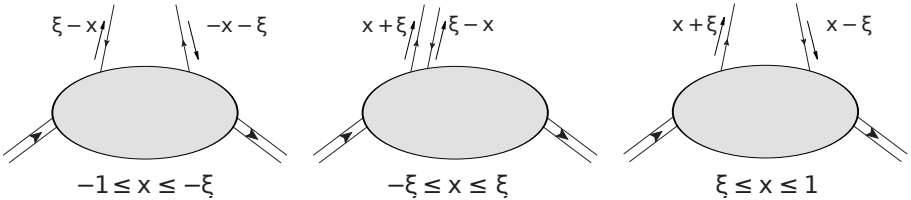

Antiquark DGLAP
$N \to N$ overlap, parton number is conserved.

ERBL
Quark–antiquark emission or absorption.

Quark DGLAP
$N \to N$ overlap, parton number is conserved.

$$X_\pi = \frac{x+\xi}{1+\xi}, \qquad X_\gamma = \frac{x-\xi}{1-\xi}, \qquad -1 \le x \le 1.$$

For this TDA, the external states in these generic support diagrams are π and γ.

Diehl, Feldmann, Jakob and Kroll, NPB 596, 33 (2001)

The TDA in DGLAP region

$$\mathcal{F}_\Gamma\big|_{x>\xi} \sim \sum_{\lambda,\bar{\lambda}} \int \frac{d^2k_\perp}{16\pi^3} \Psi^*_{\gamma,\lambda\bar{\lambda}}(X_\gamma, k_{\perp\gamma}) \mathcal{S}_\Gamma \Psi_{\pi,\lambda\bar{\lambda}}(X_\pi, k_{\perp\pi}).$$

$$X_\pi = \frac{x+\xi}{1+\xi}, \quad k_{\perp\pi} = k_\perp - \frac{1-x}{1+\xi}\frac{\Delta_\perp}{2},$$

$$X_\gamma = \frac{x-\xi}{1-\xi}, \quad k_{\perp\gamma} = k_\perp + \frac{1-x}{1-\xi}\frac{\Delta_\perp}{2}.$$

For each pion-helicity sector h:

$$A_h = e_d\,\theta(x-\xi)a_h(x,\xi,u) + (-1)^L e_u\,\theta(-x-\xi)a_h(-x,\xi,u),$$
$$V_h = e_d\,\theta(x-\xi)v_h(x,\xi,u) - e_u\,\theta(-x-\xi)v_h(-x,\xi,u).$$

$$e_u = \frac{2}{3}, \quad e_d = -\frac{1}{3}, \qquad L=0:\ h=\uparrow\downarrow, \quad L=1:\ h=\uparrow\uparrow, \qquad |x|>\xi, \quad |x|\le 1.$$

Both helicity sectors enter both currents: $A = A_{\uparrow\downarrow} + A_{\uparrow\uparrow}$ and $V = V_{\uparrow\downarrow} + V_{\uparrow\uparrow}$.

$$\mathcal{F}_{\gamma^+\gamma_5}(x,\xi,u) = \frac{e}{f_\pi}\,(\epsilon\cdot\Delta)\,A^{\pi\gamma}(x,\xi,u)\,;\ \mathcal{F}_{\gamma^+}(x,\xi,u) = \frac{ie}{P^+ f_\pi}\,\varepsilon_{\mu\nu\rho\sigma}\,n^\mu \epsilon^\nu P^\rho \Delta_\perp^\sigma V^{\pi\gamma}(x,\xi,u).$$

Constraints on a physical TDA

- **Support:** the correlator vanishes outside $x \in [-1, 1]$.
- **Polynomiality:** Mellin moments are polynomials in ξ; odd powers are allowed for a transition between different states.
- **Local-current sum rules:** after matching phase and current conventions,

$$\int_{-1}^{1} dx\, A^{\pi\gamma} = \frac{f_\pi}{m_\pi} F_A(u), \qquad \int_{-1}^{1} dx\, V^{\pi\gamma} = \frac{f_\pi}{m_\pi} F_V(u).$$

Consequences: the zeroth moments must be independent of ξ and of the QCD evolution scale.

DGLAP contribution + ERBL contribution $\longrightarrow$ one constrained full-support moment.

Covariant extension from DGLAP to ERBL

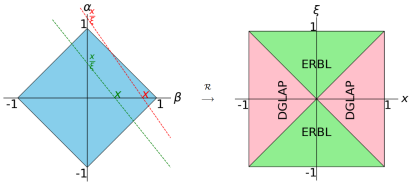

1. Reconstruct a double distribution from the outer-region overlap.
2. Use the same Radon transform in the central region.
3. Assemble the charge-weighted reflected blocks.

$$f_h(x,\xi,u) = \int_{\Omega_+} d\beta\, d\alpha\, \delta(x-\beta-\xi\alpha)\, \rho_h(\beta,\alpha,u), \qquad \Omega_+ :\ 0 \le \beta \le 1, \quad |\alpha| \le 1-\beta.$$

$$\int dx\, x^n f_h = \sum_{k=0}^{n} \binom{n}{k} \xi^k \int_{\Omega_+} d\beta\, d\alpha\, \beta^{n-k} \alpha^k \rho_h.$$

Polynomiality follows from the common DD.

Chouika et al., EPJC 77, 906 (2017), Radon geometry; Dall'Olio et al., PRD 109, 096013 (2024).

Common functions for the analytic TDAs

The overlap and its covariant extension share one normalization ($0 < \xi < 1, u \leq 0$):

$$\mathcal{N} = \frac{\sqrt{15N_c}\, f_\pi}{8\pi M}, \qquad K(x,\xi) = \mathcal{N}\frac{(1-x)^2(x+\xi)}{(1-\xi^2)^2(1+\xi)}, \qquad \zeta = \frac{-u(1-x)^2}{4M^2(1-\xi^2)}.$$

$$\ell(\zeta) = \frac{\operatorname{artanh}\sqrt{\zeta/(1+\zeta)}}{\sqrt{\zeta/(1+\zeta)}}, \qquad J_0(\zeta) = \frac{1+2\zeta-\ell/(1+\zeta)}{\zeta(1+\zeta)}, \qquad J_1(\zeta) = \frac{-1+(1+2\zeta)\ell/(1+\zeta)}{\zeta(1+\zeta)}.$$

$$J_0(0) = \frac{8}{3}, \quad J_1(0) = \frac{4}{3}.$$

ERBL polynomials at $u = 0$:

$$B_2(x,\xi) = \xi^2 - \xi^3(4+\xi) - 2x\xi[1+(4-\xi)\xi] + x^2[1+\xi(4+7\xi)],$$

$$\begin{aligned} B_4(x,\xi) = & -2\xi^4(1+\xi) + x^3\xi(1-13\xi^2) + x^2\xi^2[5+\xi(20+3\xi)] \\ & - x\xi^3[1-\xi(8+5\xi)] - x^4[3+\xi(10+11\xi)]. \end{aligned}$$

The following axial and vector slides show the building blocks and their $u = 0$ curves.

Axial TDA: formulas and helicity contributions

DGLAP: $x \geq \xi, u \leq 0$ **ERBL:** $|x| \leq \xi, u = 0$ **Curves:** $a_h/\mathcal{N}$.

Anti-aligned pion helicities

$$a^{\text{DGLAP}}_{\uparrow\downarrow} = K(1+\xi-2x)J_0(\zeta),$$

$$a^{\text{ERBL}}_{\uparrow\downarrow} = \frac{\mathcal{N}B_4}{3\xi^4(1+\xi)^3}.$$

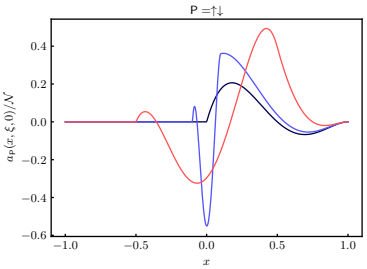

Aligned pion helicities

$$a^{\text{DGLAP}}_{\uparrow\uparrow} = K(1-\xi)J_1(\zeta),$$

$$a^{\text{ERBL}}_{\uparrow\uparrow} = -\frac{\mathcal{N}(x+\xi)B_2}{6\xi^3(1+\xi)^3}.$$

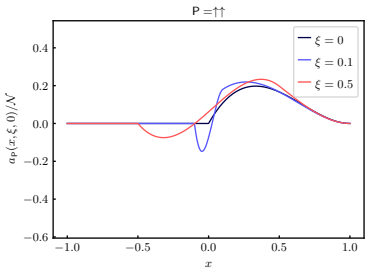

The full axial TDA at nonzero transfer

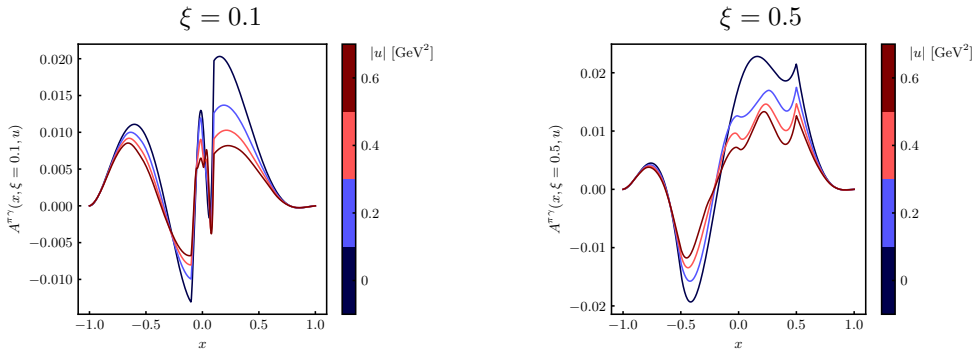

$|u| = 0, 0.2, 0.4, 0.6\ \text{GeV}^2$. Finite-$u$ ERBL values obtained from the covariant extension.

Vector TDA: formulas and helicity contributions

DGLAP: $x \geq \xi, u \leq 0$ **ERBL:** $|x| \leq \xi, u = 0$

$$u = 0: \; v_{\uparrow\downarrow} = 2v_{\uparrow\uparrow}.$$

Anti-aligned pion helicities

$$v_{\uparrow\downarrow}^{\text{DGLAP}} = K(1-\xi)J_0(\zeta),$$

$$v_{\uparrow\downarrow}^{\text{ERBL}} = -\frac{\mathcal{N}(x+\xi)B_2}{3\xi^3(1+\xi)^3}.$$

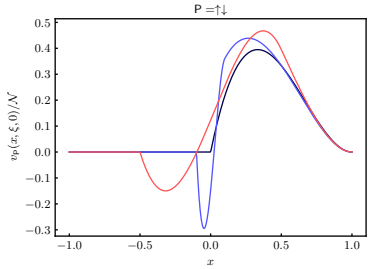

Aligned pion helicities

$$v_{\uparrow\uparrow}^{\text{DGLAP}} = K(1-\xi)J_1(\zeta),$$

$$v_{\uparrow\uparrow}^{\text{ERBL}} = -\frac{\mathcal{N}(x+\xi)B_2}{6\xi^3(1+\xi)^3}.$$

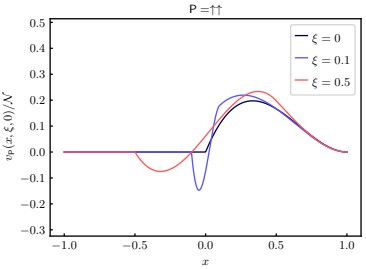

The full vector TDA at nonzero transfer

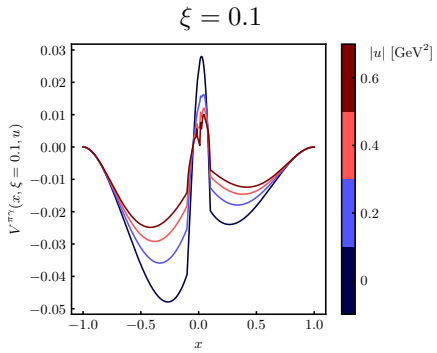

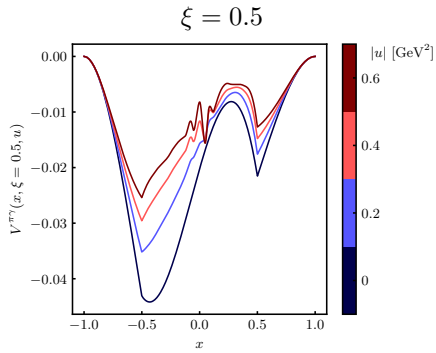

Illustration of the effect of scale evolution.

Castro et al., Fig. 4, vector panels; Sec. II D.2.

Transition form factors constrain the normalization

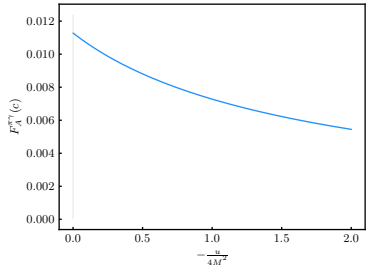

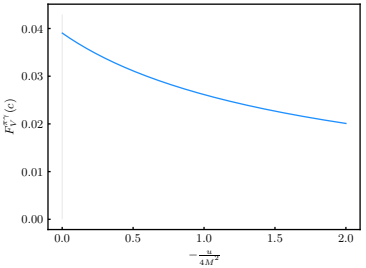

Reported magnitude at $u = 0$	Model	Experimental input	Difference
$\lvert F_A(0)\rvert$	0.0113	0.0119 ± 0.0001	about 5% low
$\lvert F_V(0)\rvert$	0.039	0.0254 ± 0.0017	about 54% high

Axial and vector $\pi \to \gamma$ transition form factors computed from our two-body models for the axial and vector TDAs. The variable c is defined as $c = -u/4M^2$.

PDG 2024.

Scale evolution at small skewness

$$\frac{\partial \mathcal{G}(x,\xi,u;\mu)}{\partial \ln \mu^2} = \int_{-1}^{1} dy\, K_{\rm NS}(x,y,\xi;\alpha_s^{\rm eff})\, \mathcal{G}(y,\xi,u;\mu), \quad \mathcal{G} = A, V.$$

- Flavor nonsinglet: no gluon mixing.
- LO evolution with APFEL++.
- $\mu_{\rm ref} = 0.331$ GeV.
- Infrared-finite effective coupling.

Axial

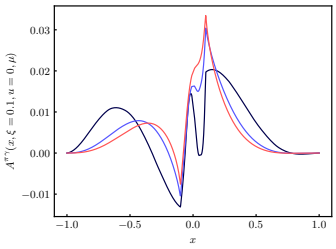

Vector

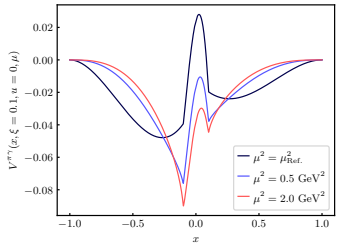

$$\xi = .1, u = 0; \mu^2 = \mu^2_{\rm ref},\ 0.5,\ 2.0\,{\rm GeV}^2.$$

Bertone et al., EPJC 82, 888 (2022).

Scale evolution at larger skewness

The same nonsinglet kernel acts over the full support. The larger ERBL interval makes the scale dependence especially visible.

- Resolution redistributes the x dependence.
- Continuous at $x = \pm\xi$; a slope cusp is allowed.
- Physical zeroth moments are conserved.
- Endpoint limits stay zero; crossover values evolve.

Axial

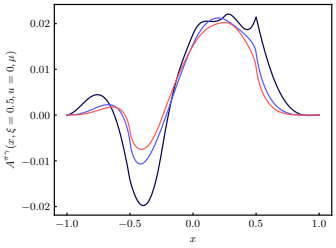

Vector

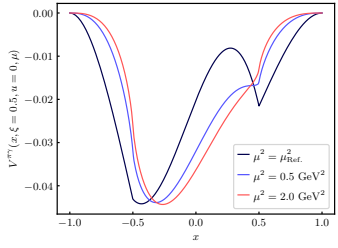

$$\xi = .5, u = 0; \mu^2 = \mu^2_{\text{ref}},\ 0.5,\ 2.0\,\text{GeV}^2.$$

From a pion target to the Sullivan cross section

$$\frac{d^5\sigma}{dt_N\, dx_\pi\, dQ^2\, dx_B\, du_\pi} \simeq f_{\pi/p}(x_\pi, t_N) \left(\frac{\alpha_{\text{em}}}{Q^2}\right)^3 \frac{x_B^\pi}{x_\pi}(1-y)\,|\mathcal{A}_L^M|^2.$$

$$\boxed{f_{\pi/p}(x_\pi, t_N) = x_\pi \frac{g_{\pi NN}^2}{8\pi^2} \frac{-t_N}{(t_N - m_\pi^2)^2} \left(\frac{\Lambda^2 - m_\pi^2}{\Lambda^2 - t_N}\right)^2}.$$

Pion emission

- $t_N = p_\pi^2$: exchanged-pion virtuality.
- x_π: proton momentum fraction carried by the pion.
- The last factor models the πNN vertex.

Hard exclusive subprocess

$$x_B^\pi \simeq \frac{x_B}{x_\pi}, \qquad \xi \simeq \frac{x_B}{2x_\pi - x_B}.$$

$\mathcal{A}_L^M$ contains the meson DA, hard coefficient and evolved TDA.

$$\frac{d^4\sigma}{dx_\pi\, dQ^2\, dx_B\, du_\pi} = \int_{-0.6\ \text{GeV}^2}^{t_0} dt_N\, \frac{d^5\sigma}{dt_N\, dx_\pi\, dQ^2\, dx_B\, du_\pi}, \qquad t_0 \simeq -\frac{x_\pi^2 m_N^2}{1 - x_\pi}.$$

Amrath, DESY-THESIS-2007-039, Secs. 3.4–3.5.

The hard amplitude and the outgoing-meson DA

$$\mathcal{A}_L^M = \frac{16\pi\alpha_s(Q)}{9Q}\int_{-1}^{1} dx \int_0^1 dz\, C^{ud}(x,z,\xi)\,\Phi_M(z,Q)\,\mathcal{G}_M(x,\xi,u,Q),$$

$$C^{ud} = \frac{e_u}{(1-z)(\xi-x-i0)} - \frac{e_d}{z(\xi+x-i0)}, \qquad \mathcal{G}_\pi = A, \quad \mathcal{G}_{\rho_L} = V.$$

Asymptotic DA used in the calculation

$$\Phi_M(z,Q) = 6 f_M z(1-z),$$

$$\int_0^1 dz\,\Phi_M = f_M, \qquad \int_0^1 dz\,\frac{\Phi_M}{z} = 3 f_M.$$

What the observable probes

- π^+ selects the axial TDA.
- ρ_L^+ selects the vector TDA.

$$\text{Im}\,\mathcal{A}_L^M = \frac{16\pi^2\alpha_s f_M}{3Q}\left[e_u\mathcal{G}_M(\xi) - e_d\mathcal{G}_M(-\xi)\right].$$

BH process is suppressed at backward scattering; the photon follows the incoming pion. Also, at the large momentum transfer BH is suppressed through the exchanged-photon propagator and the pion electromagnetic form factor.

Pion channel: an axial-TDA cross section

$$ep \to e\,\gamma\,\pi^+ n$$

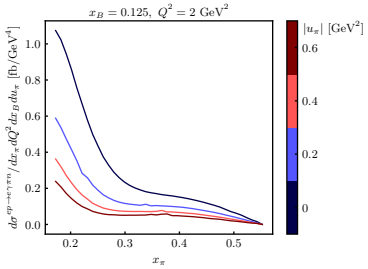

$$\frac{d^4\sigma}{dx_\pi\, dQ^2\, dx_B\, du_\pi}\ [\mathrm{fb/GeV}^4]$$

Published benchmark

E_e	22 GeV (proposed upgrade)
Q^2	2 GeV^2
x_B	0.125
$\lvert u_\pi\rvert$	0, 0.2, 0.4, 0.6 GeV^2
$g_{\pi NN}$, Λ	13.05, 0.8 GeV
t_N range	$[-0.6, t_0]$ GeV^2

The pion channel measures the squared **axial convolution**.

Small backward rates may benefit from reduced BH contamination.

Apply the cuts jointly: $s_\pi \simeq t_N + 16x_\pi - 2\ \mathrm{GeV}^2$. Requiring $s_\pi \geq 4\ \mathrm{GeV}^2$ gives $x_\pi \geq (6 - t_N)/16 \geq 0.375$, excluding part of the plotted range.

Rho channel

$$ep \to e\,\gamma\,\rho_L^+ n$$

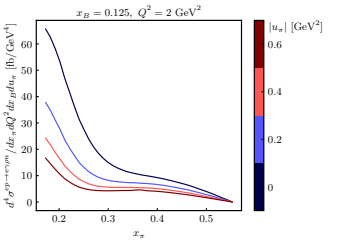

$E_e = 22\,\mathrm{GeV},\quad Q^2 = 2\,\mathrm{GeV}^2,\quad x_B = .125.$
$|u_\pi| = 0, .2, .4, .6\,\mathrm{GeV}^2;\quad$ units: fb/GeV^4.

The plotted model gives $R \sim 50$:

$$R = \frac{d\sigma_{\rho_L}}{d\sigma_\pi} \simeq \left(\frac{f_\rho}{f_\pi}\right)^2 \left|\frac{\mathcal{I}[V]}{\mathcal{I}[A]}\right|^2.$$

- Decay constants: $(f_\rho/f_\pi)^2 \sim 2.5$.
- Vector normalization excess in $F_V^{\pi\gamma}(0)$:

$$(\,0.039/0.0254\,)^2 \simeq 2.4.$$

- The relative TDA convolutions remain essential and model dependent.

$\mathcal{I}[T]$ is the TDA-dependent part of the scattering amplitude. $\mathcal{M} \propto \mathcal{I}[T], \qquad d\sigma \propto |\mathcal{M}|^2$.
$F_V^{\pi\gamma}$ **is the radiative pion–photon transition form factor.**

Conclusions and experimental questions

1. **A full-support transition model**
   Pion/photon LFWF overlaps, a covariant ERBL extension and nonsinglet evolution connect pion structure to backward exclusive production.

2. **Specific observables test specific amplitudes**
   π^+ probes $|\mathcal{I}[A]|^2$; ρ_L^+ probes $|\mathcal{I}[V]|^2$. Their ratio and its Q^2, u_π dependence test the relative normalization and shape of the TDAs.

3. **Smaller rates**
   Low probability of measuring Backward DVCS at a typical kinematic range accessible at JLab with 22 GeV electron-beams. Compared to the forward Sullivan DVCS case, the total cross-section of backward DVCS remains two orders of magnitudes below

4. **Next theory steps**
   Higher twist correction calculations.

南京大學 NANJING UNIVERSITY

非微扰物理研究所 Institute for Nonperturbative Physics



Thank You!

Abigail R. Castro · Institute for Nonperturbative Physics · Nanjing University

arcastro@nju.edu.cn

Q&A

A tested method: the pion GPD precedent

Morgado Chávez, Mezrag et al. (2022): start from a pion LFWF overlap, then extend the result covariantly to the full partonic support.

$$H_\pi\big|_{\text{DGLAP}} \sim \Psi_\pi^* \Psi_\pi \xrightarrow{\text{DD reconstruction}} H_\pi .$$

- Pion charge radius fixes $M = 318$ MeV.
- Full-support moments reproduce the pion electromagnetic form factor.
- The pion soft theorem constrains the GPD's D-term contribution.

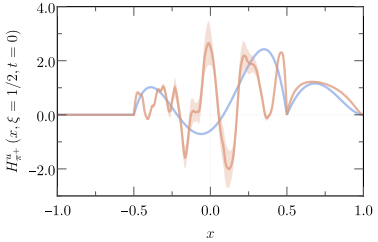

$H_\pi^u, \xi = 1/2, t = 0$, model scale.
Blue: algebraic input; brown: continuum-QCD-inspired input.

For the TDA: replace one pion wave function by a photon wave function, $\Psi_\pi^* \Psi_\pi \to \Psi_\gamma^* \Psi_\pi$.

J. M. Morgado Chávez et al., PRD 105, 094012 (2022), Fig. 5; Chouika et al., EPJC 77, 906 (2017), PLB 780, 287 (2018).

What sets the ρ_L/π cross-section hierarchy?

For the same kinematics and the asymptotic DAs used in the paper,

$$\mathcal{I}[T] = \int_{-1}^{1} dx \left[\frac{e_u}{\xi - x - i0} - \frac{e_d}{\xi + x - i0}\right] T(x, \xi, u; Q), \qquad \frac{d\sigma_{\rho_L}}{d\sigma_\pi} \simeq \left(\frac{f_\rho}{f_\pi}\right)^2 \left|\frac{\mathcal{I}[V]}{\mathcal{I}[A]}\right|^2 .$$

The sum rules involve the **radiative pion–photon transition form factors**:

$$\int_{-1}^{1} dx\,(A, V) = \frac{f_\pi}{m_\pi}(F_A^{\pi\gamma}, F_V^{\pi\gamma}), \qquad \widehat{T} = \frac{T}{\int dx\, T}.$$

$$\frac{d\sigma_{\rho_L}}{d\sigma_\pi} \simeq \underbrace{\left(\frac{f_\rho}{f_\pi}\right)^2}_{\text{decay constants}} \underbrace{\left|\frac{F_V^{\pi\gamma}(u)}{F_A^{\pi\gamma}(u)}\right|^2}_{\text{transition moments}} \underbrace{\left|\frac{\mathcal{I}[\widehat{V}]}{\mathcal{I}[\widehat{A}]}\right|^2}_{\text{relative shapes and evolution}} .$$

- The paper's "factor ~ 2" refers to the vector normalization excess: $(0.039/0.0254)^2 \simeq 2.36$ at $u = 0$.
- Separately, $(f_\rho/f_\pi)^2 \sim 2.5$. The plotted ratio ~ 50 is a model estimate; the paper's $2 \times 2.5 \times 10$ is rough bookkeeping.

Castro et al., arXiv:2504.02657, Eqs. (5), (22)–(23), (38)–(40), Fig. 7 and its discussion.

Why is Bethe–Heitler suppressed backward?

Pion channel: the real photon is radiated from either lepton leg. The electron propagator denominators are

$$D_{\text{in}} = (l - q')^2 - m_e^2 = -2l\cdot q', \qquad D_{\text{out}} = (l' + q')^2 - m_e^2 = 2l'\cdot q'.$$

The exchanged photon probes the pion current at $t_\pi = (q - q')^2$:

$$\mathcal{M}_{\text{BH}} \propto \frac{F_\pi(t_\pi)}{t_\pi} L_\mu (p_\pi + p'_\pi)^\mu, \qquad s_\pi + t_\pi + u_\pi = -Q^2 + t_N + m_\pi^2.$$

- Small $|u_\pi|$, with hard Q^2, s_π, implies $-t_\pi \simeq Q^2 + s_\pi$: the small-$|t_\pi|$ enhancement is lost and the **elastic** $F_\pi(t_\pi)$ is suppressed.
- In the massless, exactly backward limit,

$$D_{\text{in}} \simeq -\frac{s_\pi}{y_\pi}, \qquad D_{\text{out}} \simeq \frac{s_\pi(1 - y_\pi)}{y_\pi}, \qquad y_\pi = \frac{p_\pi \cdot q}{p_\pi \cdot l}.$$

  Both remain hard away from $y_\pi = 1$; lepton-collinear and soft regions require cuts.

Consequence: reduced BH contamination is expected in selected backward kinematics; its size requires an explicit calculation with the same cuts.

Amrath, DESY-THESIS-2007-039, Secs. 3.3.2.2–3.3.2.3; Amrath–Diehl–Lansberg, EPJC 58, 179 (2008), Eqs. (32)–(34); Castro et al., Sec. III.

Why does the final meson select the TDA?

For a longitudinal virtual photon, the massless leading-twist hard part couples to the outgoing meson's collinear projector:

$$\mathcal{P}_\pi \propto \not{p}'_M \gamma_5 \, \Phi_\pi(z), \qquad \mathcal{P}_{\rho_L} \propto \not{p}'_M \, \Phi_{\rho_L}(z).$$

Final meson	TDA current	Leading-twist channel
π^+	$\bar{d}\gamma^+\gamma_5 u$	$\Phi_\pi \otimes H \otimes A^{\pi\gamma}$
ρ_L^+	$\bar{d}\gamma^+ u$	$\Phi_{\rho_L} \otimes H \otimes V^{\pi\gamma}$

Why do the mixed projections vanish? A single-γ_5 trace produces a Levi-Civita tensor. In the collinear hard part, all external vectors lie in the span of two lightlike directions, so

$$\epsilon_{\mu\nu\rho\sigma} n^\mu \bar{n}^\nu a^\rho b^\sigma = 0, \qquad a, b \in \text{span}\{n, \bar{n}\}.$$

Chiral-odd tensor TDAs cannot pair with these chiral-even meson DAs.

A separate issue: both pion LFWF helicity sectors contribute to both TDAs: $A = A_{\uparrow\downarrow} + A_{\uparrow\uparrow}, V = V_{\uparrow\downarrow} + V_{\uparrow\uparrow}$.

Castro et al., Eqs. (3)–(4), (15), (39); Lansberg–Pire–Szymanowski, PRD 73, 074014 (2006), Secs. 3.2 and 4.1.

Backup: Fock-Space States

At fixed light-front time, the state is a sum of amplitudes for different constituent sectors. Here $\otimes$ includes momentum integration and spin/color sums.

$$|\pi^+\rangle = \Psi_2^\pi \otimes |u\bar{d}\rangle + \Psi_3^\pi \otimes |u\bar{d}g\rangle + \Psi_4^\pi \otimes |u\bar{d}q\bar{q}\rangle + \cdots ,$$

$$|\gamma_\lambda\rangle = \sqrt{Z_3}\,|\gamma_\lambda\rangle_{\text{bare}} + \sum_f \Psi_{2,f}^{\gamma,\lambda} \otimes |f\bar{f}\rangle + \sum_f \Psi_{3,f}^{\gamma,\lambda} \otimes |f\bar{f}g\rangle + \cdots .$$

Pion: a two-body valence input

$|u\bar{d}\rangle$ is the lowest sector. Higher sectors also include $|u\bar{d}gg\rangle$ and additional sea pairs.

$$J_z = 0 : \quad \lambda + \bar{\lambda} + L_z = 0.$$

Anti-aligned helicities have $L_z = 0$; aligned helicities require $k_x \mp ik_y$ orbital factors.

Photon: pointlike and resolved components

The elementary photon term and its $q\bar{q}$ component are distinct. The model's pointlike $ee_f\gamma^\mu$ vertex generates the lowest resolved $f\bar{f}$ light-front amplitude.

The overlap calculation retains Ψ_2^π and Ψ_2^γ; it does not determine every Fock component of either physical state.

Brodsky, Pauli and Pinsky, Phys. Rep. 301, 299 (1998); Castro et al., PRD 112, 034009 (2025), Sec. II; Ball, Braun and Kivel, NPB 649, 263 (2003).

Backup: What the Fock overlaps determine

For $\xi = (p_\pi^+ - q'^+)/(2P^+) > 0$, the bilocal quark operator probes

$$\mathcal{F}_\Gamma \sim \langle \gamma | \bar{d}(-z/2)\, \Gamma\, u(z/2) | \pi^+ \rangle .$$

DGLAP: same particle number

$$|x| > \xi : \qquad \mathcal{F}_\Gamma \sim \sum_n (\Psi_n^\gamma)^* \otimes \Psi_n^\pi .$$

The operator removes and reinserts a quark or antiquark; the spectators match. The retained $2 \to 2$ overlap gives the valence contribution in this region.

ERBL: a quark–antiquark pair

$$|x| < \xi : \qquad \mathcal{F}_\Gamma \sim \sum_n (\Psi_n^\gamma)^* \otimes \Psi_{n+2}^\pi .$$

For this sign of ξ, the pion side supplies the pair. In the resolved-photon sector an example is $4 \to 2$; the two-body overlap alone does not determine it.

The paper obtains the central region through a covariant double-distribution extension constrained by the DGLAP result and polynomiality.

Amplitude interpretation: $\Psi_\gamma^* \Psi_\pi$ connects different external states; it is not a pion probability density.

Diehl, Feldmann, Jakob and Kroll, NPB 596, 33 (2001), erratum B605, 647; Chouika et al., EPJC 77, 906 (2017); Castro et al., Sec. II.

Backup: Experimental Feasibility and Facilities

Facility status checked 22 October 2026

Facility	Status	Role in this study
JLab 12 GeV	Operating CEBAF	Related backward-meson program, e.g. E12-20-007; a different channel from Sullivan DVCS.
JLab 22 GeV	Proposed upgrade; R&D	The $E_e = 22$ GeV curves are model projections.
EIC / ePIC	Future collider; CD-3B procurement approved (2026)	Sullivan neutron tagging needs channel-specific acceptance and background studies.

What is predicted

$$\frac{d^4\sigma}{dx_\pi\, dQ^2\, dx_B\, du_\pi} \quad [\mathrm{fb/GeV}^4],$$

after integrating t_N; the displayed benchmark uses $Q^2 = 2\,\mathrm{GeV}^2$, $x_B = 0.125$.

$$N = \mathcal{L}_{\mathrm{int}} \int_{\mathrm{cuts}} d\Phi\, \frac{d\sigma}{d\Phi}\, \mathcal{A}\, \epsilon\, \mathcal{B}.$$

What an experimental study must resolve

- Neutron acceptance, resolution and exclusivity with simultaneous hard-regime cuts.
- $\rho_L^+ \to \pi^+\pi^0$: decay-angle analysis and polarization separation.
- Signal, Bethe–Heitler and other backgrounds folded with acceptance and efficiency.

JLab facility/experiment pages; Rossi–Shepherd update, 27 Jul. 2026; BNL CD-3B announcement, 6 Feb. 2026; Castro et al., Fig. 7; Morgado Chávez et al., PRL 128, 202501 (2022).

2005–2007: fitted constraints and spectral dynamics

Tiburzi (2005): realistic DD ansatz

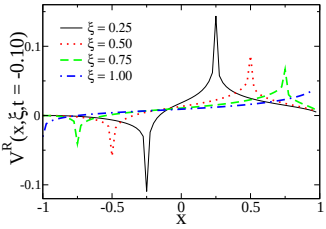

Pion and hadronic-photon PDFs constrain the shape.
$F_V(0)$ and $F_A(0)$ are **fitted inputs**.
Shown: $t = -0.10\,\mathrm{GeV}^2$, $\mu^2 = 0.40\,\mathrm{GeV}^2$.

Broniowski–Ruiz Arriola (2007)

Spectral quark model: $8\pi^2 V_{\text{direct}}(x, \zeta, 0)$

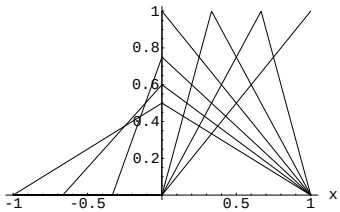

Covariant quark loop $\longrightarrow$ analytic DDs.
Chiral limit; $M_V = 0.77\,\mathrm{GeV}$; low model scale.
Native (x, ζ) and direct graph, before isospin assembly.

Comparison different input constructions; these native plots are not yet the same charged-channel TDA in common coordinates.

B. C. Tiburzi, PRD 72, 094001 (2005), Sec. IV, Eqs. (34)–(37), Fig. 4; hep-ph/0508112. W. Broniowski and E. Ruiz Arriola, PLB 649, 49 (2007), Eqs. (3), (14)–(21), Fig. 2; hep-ph/0701243.

2007: NJL and overlap models have different ingredients

Courtoy–Noguera: covariant NJL

$t = 0$; red curve: $\xi = 0.5$

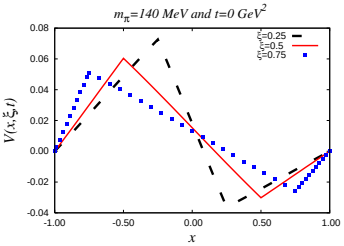

Castro et al.: LFWF overlap

$\xi = 0.5$; darkest curve: $u = 0$

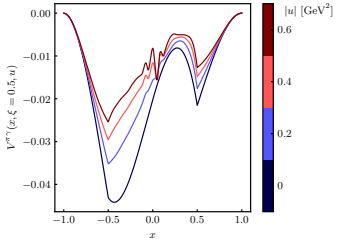

NJL + Pauli–Villars: both regions arise directly.

Two-body overlap; ERBL from double distributions.

Axial difference: NJL retains a nonresonant $q\bar{q}$ rescattering contribution after subtracting the pion pole; it matters in ERBL.

Native conventions shown: the printed antiquark signs differ. A quantitative vector overlay needs that comparison resolved first.

A. Courtoy and S. Noguera, PRD 76, 094026 (2007), Eqs. (4)–(7), (12), (16)–(23), (33), Figs. 4 and 6; arXiv:0707.3366. Castro et al., PRD 112, 034009 (2025), Eq. (16), Fig. 4; arXiv:2504.02657v1.

2009–2013: a conserved current changes the result

Kotko–Praszałowicz: momentum-dependent mass and nonlocal vertices,

$$\Gamma^\mu(k,p) = \gamma^\mu - \frac{(k+p)^\mu}{k^2-p^2}\,[M(k)-M(p)].$$

Vector: anomaly normalization restored

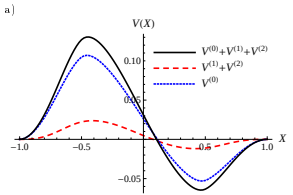

Axial: a negative current correction

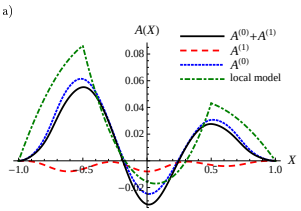

Shown: $\xi = 0.5$, $t = -0.1\,\text{GeV}^2$, $M = 350\,\text{MeV}$, $n = 1$; chiral limit.
Difference: these dressed vertices add physics absent from a constant-mass, bare-photon vertex. Here $F_A(0) = 0.0168$ and $F_V(0) \simeq 0.027$.

P. Kotko and M. Praszałowicz, PRD 80, 074002 (2009), Eqs. (3)–(8), (29), (35)–(36), Figs. 1a and 2a, Table II; arXiv:0907.4044. P. Kotko, Acta Phys. Pol. B Proc. Suppl. 6, 195 (2013), Fig. 2, Table I; DOI:10.5506/APhysPolBSupp.6.195.

2024: proper-time NJL gives a different form-factor pattern

Zhang–Wu: local NJL with proper-time UV and IR cutoffs; pion and kaon TDAs.

Zhang–Wu: F_V **and** F_A

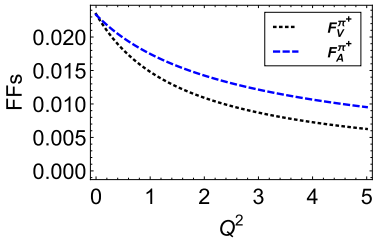

$F_V(0) = 0.0234$, $F_A(0) = 0.0233$

Castro et al.: F_V

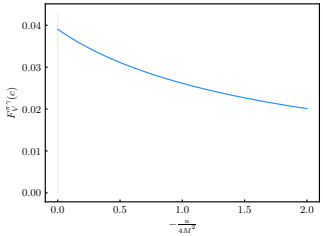

$F_V(0) = 0.039$; $F_A(0) = 0.0113$ in the axial sector

Match the horizontal variables: $Q_T^2 = -t$ on the left; $c = -u/(4M^2)$ on the right, with $M = 0.318$ GeV.
At the same pion–photon transfer, $t = u$ and $Q_T^2 = 4M^2 c$.

The NJL axial form factor is close to its vector one; this differs from Castro's reported $F_A/F_V \simeq 0.29$.

J.-L. Zhang and J. Wu, Chinese Phys. C 48, 083106 (2024), Table 1, Eqs. (32)–(34), Fig. 5 left; DOI:10.1088/1674-1137/ad2b54; arXiv:2402.12757. Castro et al., PRD 112, 034009 (2025), Fig. 2b, Eqs. (22)–(23).

What can be compared quantitatively now?

Reported charged-pion radiative form factors at zero transfer

Model / reference	$F_V(0)$	$F_A(0)$	Status
Tiburzi (2005), realistic ansatz	0.0259	0.0115	Fitted inputs
Spectral quark model (2007)	$\simeq 0.026$	$\simeq 0.026$	Chiral prediction
Courtoy–Noguera (2007)	0.0242	0.0239	NJL prediction
Kotko–Praszałowicz (2009)	$\simeq 0.027$	0.0168	$M = 350$ MeV, $n = 1$
Zhang–Wu (2024)	0.0234	0.0233	NJL prediction
Castro et al. (2025)	0.039	0.0113	Overlap prediction
PDG 2024, as quoted by Castro	0.0254 ± 0.0017	0.0119 ± 0.0001	Experimental reference

There is no common "50% high in V, 5% agreement in A" pattern.

For TDA or cross-section comparisons, first match the charged operator and antiquark signs, ξ, $t_{\mathrm{TDA}} = u_\pi$, input/evolved scale, and axial pole subtraction.

Then use the same hard kernel, meson DA, Sullivan flux and cuts. The earlier model papers do not supply Castro's matched 22 GeV Sullivan observable.

Tiburzi: Sec. IV; Broniowski–Ruiz Arriola: Eqs. (21), (26); Courtoy–Noguera: Sec. IV; Kotko–Praszałowicz: Table II, Eq. (39); Zhang–Wu: Sec. II.C.2; Castro: Eqs. (22)–(23). All entries are the numbers reported by the cited articles, with fitted inputs explicitly marked.

Pion GPD precedent: distributions and form factors

Morgado Chávez, Mezrag et al., PRD 105, 094012 (2022)

$$H_\pi^u\big|_{x>\xi} = \int \frac{\mathrm{d}^2 \boldsymbol{k}_\perp}{16\pi^3} \Psi_\pi^*(\mathrm{out})\Psi_\pi(\mathrm{in}) \xrightarrow{\text{DD inversion + soft-pion constraint}} H_\pi^u \text{ on } [-1,1].$$

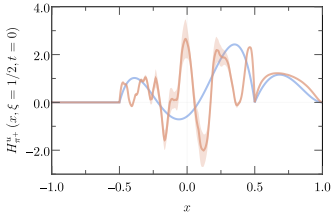

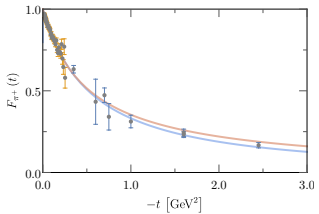

Full support: $\xi = 1/2$, $t = 0$, at the model scale.
The soft-pion theorem fixes the GPD's D-term ambiguity; the ERBL shape remains model dependent.

Electromagnetic form factor: agreement with data, especially for $|t| \lesssim 1$ GeV^2.
$M = 318$ MeV is fixed by the pion charge radius.

Blue: algebraic input, $q_\pi = 30x^2(1-x)^2$. Brown: numerical PDF input from continuum QCD/BSE studies.

J. M. Morgado Chávez et al., Phys. Rev. D **105**, 094012 (2022), Figs. 5–6, Eqs. (22), (31)–(33), (43)–(44). Overlap–DD predecessors: N. Chouika et al., EPJC **77**, 906 (2017); PLB **780**, 287 (2018).

GPD evolution and the comparison with $\pi \to \gamma$ TDAs

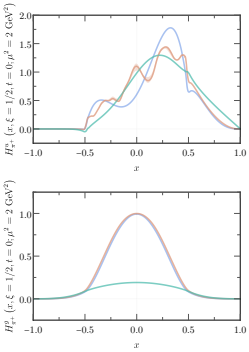

$\mu^2 = 2\,\mathrm{GeV}^2, \xi = 1/2, t = 0.$
Blue: algebraic; brown: numerical;
green: phenomenological xFitter/RDDA.
Top: H^u_π; bottom: H^g_π.

	Pion GPD	**Pion–photon TDA**
Matrix element	$\langle \pi \vert \bar{q}\gamma^+ q \vert \pi \rangle$	$\langle \gamma \vert \bar{d}\,\Gamma u \vert \pi^+ \rangle$
Overlap	$\Psi^*_\pi \Psi_\pi$	$\Psi^*_\gamma \Psi_\pi$
First moment	Electromagnetic F_π	Transition F_V, F_A
Evolution	Singlet mixes with gluons	Nonsinglet; no gluon mixing
Observable	Forward pion DVCS	Backward pion DVCS

GPD result: sizeable gluon distributions and strong NLO gluon effects in pion-DVCS Compton form factors.

TDA check in Castro et al.:

	$F_A^{\pi\gamma}(0)$	$F_V^{\pi\gamma}(0)$
model	0.0113	0.039
PDG 2024, quoted	0.0119	0.0254

Morgado Chávez et al., PRD **105**, 094012 (2022), Fig. 9 and Sec. VI. Castro et al., arXiv:2504.02657v1, Secs. II–III; Eqs. (22)–(23); PDG 2024 values as quoted there.

Backup: forward Sullivan benchmark (ADL 2008)

Same final state, $ep \to e\gamma\pi^+ n$, in **near-forward** pion-DVCS kinematics.

Beam and integration cuts

$$E_e = 11\,\text{GeV}, \qquad y \le 0.85,$$

$$Q^2 \ge 2, \quad s_\pi \ge 4, \quad |t_N| \le 0.3, \quad |t_\pi| \le 0.7 \quad [\text{GeV}^2].$$

$t_N = p_\pi^2; t_\pi = (q - q')^2$. No additional $M_{\pi n}$ cut in this benchmark.

Integrated rates: model 1

Contribution	σ [fb]
Pure DVCS	0.88
Bethe–Heitler	18.4
Interference (e^- beam)	-0.18

Acceptance cuts: energies in GeV; polar angles relative to the beam.

Electron: $E'_e > 0.5$, $8^\circ < \theta_e < 45^\circ$ Photon: $E_\gamma > 0.1$, $2^\circ < \theta_\gamma < 40^\circ$ Pion: $E_\pi > 0.2$, $5^\circ < \theta_\pi < 135^\circ$

No matched numerical ratio: these integrated forward rates are in fb. Castro's 22 GeV backward curves show $d^4\sigma/(dx_\pi\, dQ^2\, dx_B\, du_\pi)$ in fb/GeV^4. Matching energy, cuts and differential measure requires a new calculation.

D. Amrath, M. Diehl and J.-P. Lansberg, EPJ C 58, 179–192 (2008), Table 1 and Eqs. (45), (49), (50); arXiv:0807.4474. DOI: 10.1140/epjc/s10052-008-0769-1.

Why the zero-transfer limits matter numerically

On main slide 14, $\zeta = -u(1-x)^2/[4M^2(1-\xi^2)]$. Thus $u \to 0$ gives $\zeta \to 0$. The two scalar overlap functions have removable $0/0$ forms:

$$J_0(\zeta) = \frac{1 + 2\zeta - \ell(\zeta)/(1+\zeta)}{\zeta(1+\zeta)}, \qquad J_1(\zeta) = \frac{-1 + (1+2\zeta)\ell(\zeta)/(1+\zeta)}{\zeta(1+\zeta)}.$$

Their series give finite limits:

$$J_0(\zeta) = \frac{8}{3} - \frac{16}{5}\zeta + O(\zeta^2), \qquad J_1(\zeta) = \frac{4}{3} - \frac{32}{15}\zeta + O(\zeta^2).$$

- These are derived limits of the displayed analytic functions, not extra fitted constants.
- Use the limits or a series near zero to avoid subtracting nearly equal numbers.
- They explain $v_{\uparrow\downarrow} = 2v_{\uparrow\uparrow}$ at $u = 0$ in this particular algebraic model.

Taylor expansion of the scalar regrouping of Castro et al., Eqs. (18)–(21). $\ell(\zeta) = \operatorname{artanh}\sqrt{\zeta/(1+\zeta)}/\sqrt{\zeta/(1+\zeta)}$.

Published TDA model and pion-GPD framework

[1] A. R. Castro, C. Mezrag, J. M. Morgado Chávez and B. Pire
Backward DVCS in a Sullivan process. Phys. Rev. D 112, 034009 (2025). arXiv:2504.02657

[2] J. M. Morgado Chávez et al.
Pion generalized parton distributions: A path toward phenomenology. Phys. Rev. D 105, 094012 (2022). arXiv:2110.06052

[3] J. M. Morgado Chávez et al.
Accessing the pion 3D structure at U.S. and China electron-ion colliders. Phys. Rev. Lett. 128, 202501 (2022). arXiv:2110.09462

[4] B. Pire and L. Szymanowski
Hadron annihilation into two photons and backward dVCS in the scaling regime of QCD. Phys. Rev. D 71, 111501 (2005). hep-ph/0411387

[5] M. Diehl, T. Feldmann, R. Jakob and P. Kroll
The overlap representation of skewed quark and gluon distributions. Nucl. Phys. B 596, 33 (2001). arXiv:hep-ph/0009255

Pion wave functions and the covariant extension

[6] C. Mezrag, L. Chang, H. Moutarde, C. D. Roberts, J. Rodríguez-Quintero, F. Sabatié and S. M. Schmidt
Sketching the pion's valence-quark generalised parton distribution. PLB 741, 190–196 (2015). DOI: 10.1016/j.physletb.2014.12.027

[7] C. Mezrag, H. Moutarde and J. Rodríguez-Quintero
From Bethe-Salpeter wave functions to generalised parton distributions. Few-Body Syst. 57, 729 (2016). arXiv:1602.07722

[8] N. Chouika, C. Mezrag, H. Moutarde and J. Rodríguez-Quintero
A Nakanishi-based model illustrating the covariant extension of the pion GPD overlap representation and its ambiguities. PLB 780, 287–293 (2018). 1711.11548

[9] N. Chouika, C. Mezrag, H. Moutarde and J. Rodríguez-Quintero
Covariant extension of the GPD overlap representation at low Fock states. Eur. Phys. J. C 77, 906 (2017). arXiv:1711.05108

[10] P. Dall'Olio et al.
Unraveling generalized parton distributions through Lorentz symmetry and partial DGLAP knowledge. Phys. Rev. D 109, 096013 (2024). arXiv:2401.12013

Evolution, photon input and the Sullivan process

[11] V. Bertone, H. Dutrieux, C. Mezrag, J. M. Morgado and H. Moutarde
Revisiting evolution equations for generalised parton distributions. Eur. Phys. J. C 82, 888 (2022). arXiv:2206.01412

[12] P. Ball, V. M. Braun and N. Kivel
Photon distribution amplitudes in QCD. Nucl. Phys. B 649, 263 (2003). arXiv:hep-ph/0207307

[13] J. D. Sullivan
One-pion exchange and deep-inelastic electron-nucleon scattering. Phys. Rev. D 5, 1732 (1972). DOI

[14] D. Amrath, M. Diehl and J.-P. Lansberg
Deeply virtual Compton scattering on a virtual pion target. Eur. Phys. J. C 58, 179–192 (2008). 0807.4474

[15] D. Amrath
Exclusive Scattering off the Deuteron. Ph.D. thesis, Universität Hamburg (2007), DESY-THESIS-2007-039. DOI: 10.3204/DESY-THESIS-2007-039

Minkowski dynamics, diagrams and project records

[16] T. Frederico, E. Pace, B. Pasquini and G. Salmè
Pion generalized parton distributions with covariant and light-front constituent quark models. Phys. Rev. D 80, 054021 (2009). arXiv:0907.5566

[17] E. Ydrefors, W. de Paula, J. H. Alvarenga Nogueira, T. Frederico and G. Salmè
Pion electromagnetic form factor with Minkowskian dynamics. Phys. Lett. B 820, 136494 (2021). arXiv:2106.10018

[18] C. Mezrag
Lecture on Generalised Partons Distributions of Pseudo-Goldstone bosons and the nucleon. School of Physics of Baryons, 21 Oct. 2021, slide 32. Lecture PDF

[19] ARC TDA project report
TDA FMM. Checkpoint supplied 19 October 2026; especially Secs. 17 and 23.

[20] ARC TDA project report
ARC TDA Project Check. Checkpoint supplied 28 September 2026; normalization status updated by TDA FMM.

[21] ARC TDA archived presentations
`main_TDA_BSE.tex` and `ARC_TDA_BSE_Frederico_Presentation.tex`, 1 Oct. 2026. Exact stored profiles; provenance and numerical cross-checks in `data/`.

Pion–photon TDA models: original calculations

[22] B. C. Tiburzi
Estimates for Pion-Photon Transition Distributions. Phys. Rev. D 72, 094001 (2005). hep-ph/0508112

[23] W. Broniowski and E. Ruiz Arriola
Pion-photon Transition Distribution Amplitudes in the Spectral Quark Model. Phys. Lett. B 649, 49–56 (2007). hep-ph/0701243

[24] A. Courtoy and S. Noguera
Pion-photon transition distribution amplitudes in the Nambu–Jona-Lasinio model. Phys. Rev. D 76, 094026 (2007). arXiv:0707.3366

[25] P. Kotko and M. Praszałowicz
Pion-to-photon transition distribution amplitudes in the non-local chiral quark model. Acta Phys. Polon. B 40, 123–152 (2009). arXiv:0803.2847

Nonlocal currents, recent NJL results and factorization

[26] P. Kotko and M. Praszałowicz
Covariant nonlocal chiral quark model and pion-photon transition distribution amplitudes. Phys. Rev. D 80, 074002 (2009). arXiv:0907.4044

[27] P. Kotko
Pion-photon transition distribution amplitudes in non-local chiral quark model. Acta Phys. Polon. B Proc. Suppl. 6, 195–200 (2013). DOI: 10.5506/APhysPolBSupp.6.195

[28] J.-L. Zhang and J. Wu
Pion-photon and kaon-photon transition distribution amplitudes in the Nambu–Jona-Lasinio model. Chinese Phys. C 48, 083106 (2024). arXiv:2402.12757

[29] J. C. Collins and A. Freund
Proof of factorization for deeply virtual Compton scattering in QCD. Phys. Rev. D 59, 074009 (1999). hep-ph/9801262

Channel selection, Fock states and facility status

[30] J.-P. Lansberg, B. Pire and L. Szymanowski
Exclusive meson pair production in $\gamma^*\gamma$ scattering at small momentum transfer. Phys. Rev. D 73, 074014 (2006). hep-ph/0602195

[31] S. J. Brodsky, H.-C. Pauli and S. S. Pinsky
Quantum Chromodynamics and Other Field Theories on the Light Cone. Phys. Rep. 301, 299–486 (1998). hep-ph/9705477

[32] P. Rossi and M. Shepherd, Jefferson Lab
Development of the CEBAF 22 GeV Upgrade, 27 July 2026. Official project update

[33] Brookhaven National Laboratory
DOE Approves Next Phase of Funding for Electron-Ion Collider, 6 February 2026. CD-3B announcement

[34] Jefferson Lab approved experiment E12-20-007
Backward-angle Exclusive π^0 Production above the Resonance Region. Experiment entry